INFECTION AND IMMUNITY, Sept. 2009, p. 3651–3660 Vol. 77, No. 9
0019-9567/09/$08.00+0 doi:10.1128/IAI.00408-09

Real-Time Observation of *Listeria monocytogenes*-Phagocyte Interactions in Living Zebrafish Larvae▽†

Jean-Pierre Levraud,[1,2]* Olivier Disson,[3,4] Karima Kissa,[1,2] Isabelle Bonne,[6]§ Pascale Cossart,[7,8,9] Philippe Herbomel,[1,2]‡ and Marc Lecuit[3,4,5]‡

Macrophages et Développement de l'Immunité, Institut Pasteur, Paris, France[1]; CNRS URA2578, Paris, France[2]; Microorganismes et Barrières de l'Hôte, Institut Pasteur, Paris, France[3]; Inserm Avenir U604, Paris, France[4]; Université Paris-Descartes, Paris, France[5]; Plate-Forme de Microscopie Ultrastructurale, Institut Pasteur, Paris, France[6]; Interactions Bactéries-Cellules, Institut Pasteur, Paris, France[7]; Inserm U604, Paris, France[8]; and INRA USC2020, Paris, France[9]

Received 12 April 2009/Returned for modification 20 May 2009/Accepted 16 June 2009

The zebrafish, *Danio rerio*, has become a popular vertebrate model for the study of infections, mainly because of its excellent optical accessibility at the embryonic and larval stages, when the innate immune system is already effective. We have thus tested the susceptibility of zebrafish larvae to the human pathogen *Listeria monocytogenes*, a gram-positive, facultative, intracellular bacterium that is known to survive and multiply in professional phagocytes and that causes fatal meningitis and abortions. Intravenous injection of early zebrafish larvae resulted in a progressive and ultimately fatal infection. Blood-borne *L. monocytogenes* bacteria were quickly trapped and engulfed by macrophages, an event that, for the first time, could be captured in vivo and in real time. Granulocytes also participated in the innate immune response. As in mammals, bacteria could escape the macrophage phagosome in a listeriolysin-dependent manner and accessed the cytosol; this event was critical for bacterial virulence, as listeriolysin-deficient bacteria were completely avirulent. Actin comet tails and protrusions were observed, suggesting cell-to-cell spread; these phenomena also played a role in virulence in zebrafish larvae, as *actA*-deficient bacteria were attenuated. These results demonstrate the relevance of the genetically tractable and optically accessible zebrafish model for the study of *L. monocytogenes* pathogenesis and particularly for the dissection of its interactions with phagocytes in vivo, a key factor of *L. monocytogenes* virulence.

Listeria monocytogenes is a facultative, intracellular, gram-positive bacterium that may infect humans following the ingestion of contaminated food. *L. monocytogenes* has the ability to cross the human gut epithelium and then to disseminate to inner organs such as liver and spleen. Although most bacteria appear to be quickly killed by professional phagocytes, some may lyse the phagosomal membrane and access the cytosol of macrophages, where they can replicate. In immunocompetent individuals, the activation of macrophages and neutrophils relayed by specific T-cell-mediated immunity leads to the eradication of bacteria and recovery. In contrast, in pregnant women and immunocompromised hosts, infection may last and disseminate, with bacteria crossing the placental barrier and the blood-brain barrier (BBB), causing deadly forms of listeriosis (reviewed in reference 21).

L. monocytogenes was first used as a model to investigate the adaptive immune response to facultative intracellular bacteria (27, 32). Virulence mechanisms of *L. monocytogenes* have also been largely studied, leading to the discovery of key bacterial virulence factors, such as listeriolysin (encoded by *hly*), which is involved in escape of *L. monocytogenes* from the vacuole (9), and *actA*, which mediates actin-based intracellular motility and cell-to-cell spread of *L. monocytogenes* (18). *L. monocytogenes* also expresses two proteins that mediate species-specific adhesion to and invasion of nonphagocytic cells: internalin (InlA) promotes entry into cultured human cells of epithelial origin following its interaction with E-cadherin (29), while InlB promotes entry after the engagement of Met in many cell types (36). Among the in vivo models of *L. monocytogenes* infection, the mouse has been the most used, especially for exploring immune responses to *L. monocytogenes*. However, the mouse is poorly permissive to orally acquired and fetoplacental listeriosis since mouse E-cadherin is not recognized by InlA (22). In contrast, in animal models permissive to both InlA and InlB internalization pathways, such as the gerbil and a knock-in mouse line expressing a "humanized" E-cadherin enabled to interact with InlA, *L. monocytogenes* efficiently crosses the intestinal and placental barriers, which thus appears to reproduce the characteristics of human disease (6).

Although listeriosis is one of the best-characterized intracellular bacterial infections, several key events in the course of this infection remain poorly understood, as almost all our current knowledge is derived from in vitro systems or from examinations of fixed samples. Recently, two-photon microscopy has allowed the in vivo observation of the initiation of the T-cell response in explanted mouse spleens; *L. monocytogenes* has to be transported to the T-cell zone of the white pulp, where specific $CD8^+$ cells then cluster around infected dendritic cells (1). However, in that study, in vivo imaging was limited to host cells; bacteria were detectable only on cryosec-

* Corresponding author. Mailing address: Macrophages et Développement de l'Immunité, Institut Pasteur, 25 rue du Docteur Roux, 75015 Paris, France. Phone: (33) 1 45 68 85 84. Fax: (33) 1 45 68 89 21. E-mail: jean-pierre.levraud@pasteur.fr.

† Supplemental material for this article may be found at http://iai.asm.org/.

‡ P.H. and M.L. contributed equally.

§ Present address: Cell Imaging Lab, SF VA Medical Center, San Francisco, CA.

▽ Published ahead of print on 22 June 2009.

tions, leaving open the question of how *L. monocytogenes* was transported to these zones. Visualization of early events of infection in the blood compartment (e.g., bacterial sensing and trapping) is hardly achievable in the mouse and has in fact not been investigated in vivo so far. Moreover, although an increasing number of genetically modified mouse lines is available, high-throughput screens in more versatile animal models are needed to discover new genes involved in immune responses. It thus appears timely to study *L. monocytogenes* in alternative nonmammalian models that offer powerful tools for imaging and genetic engineering, such as the transparent nematode *Caenorhabditis elegans*; the fruit fly, *Drosophila melanogaster*; or the zebrafish, *Danio rerio* (19). A model of *L. monocytogenes* infection of *Drosophila* has been established (28), and subsequent advances in our understanding of the link between innate immune recognition and autophagy have been achieved with this model (40). The larval zebrafish is another attractive model: as a vertebrate, its vascular and innate immune systems are much closer to those of mammals than those of the fruit fly while retaining the advantages of genetic tractability and excellent optical accessibility; macrophages and granulocytes, notably, are readily observable in detail by video-enhanced differential interference contrast (DIC) microscopy (13, 24). In addition, whereas flies lack an adaptive immune system, adult fish possess B and T lymphocytes; however, adult zebrafish are much less experimentally tractable than embryos or early larvae, since (i) they are thicker and less transparent, making microscopic observation less easy, and (ii) gene knockdown or overexpression based on the injection of antisense morpholinos or synthetic mRNA at the one-cell stage only lasts for a few days. Models of infection with *Mycobacterium marinum*, a natural pathogen of zebrafish (3, 5); *Salmonella enterica* serovar Typhimurium, a human and mouse gram-negative pathogenic bacterium (38); or the gram-positive opportunistic pathogen of humans and cattle *Staphylococcus aureus* (34) have been successfully developed using larval zebrafish. We therefore decided to study the model pathogen *Listeria monocytogenes* and to investigate the outcome of experimental listeriosis in zebrafish larvae.

Although *L. monocytogenes* is known to contaminate seafood including fish products (14), it is not clear if fish are actually infected in the wild and develop listeriosis. The virulences of various *Listeria* species were previously tested using the adult zebrafish by Menudier et al. (30), who concluded that it was very resistant to *L. monocytogenes* infection. However, those experiments were carried out at 22°C, a temperature that is far from optimal for the expression of *Listeria* virulence genes (16). Zebrafish are tropical fish, and we could thus test the outcome of experimental infection of early zebrafish larvae at 28°C, the standard laboratory temperature. We have established that under these conditions, wild-type *L. monocytogenes* is highly virulent following intravenous (i.v.) inoculation, in contrast with its nonpathogenic relative, *Listeria innocua*. As in mammals, virulent *L. monocytogenes* bacteria escape from the phagosome and invade the cytosol of macrophages, where they induce the formation of actin-based comet tails. These major virulence mechanisms involve the same bacterial factors as those in mammalian systems, since, as in the i.v. infected mouse, *hly* deletion mutants are found to be completely avirulent and *actA* deletion mutants are found to be strongly attenuated. In this new experimental model, we could also image, for the first time in vivo, noninvasively, and in real time, critical host-bacterium interaction events, including the capture and phagocytosis of blood-borne bacteria.

MATERIALS AND METHODS

Fish. Wild-type AB purchased from the Zebrafish International Resource Center (Eugene, OR), or their F1 offspring, and *nacre* mutants (26) were raised in our facility. Eggs were obtained by marble-induced spawning, bleached according to protocols described in *The Zebrafish Book* (39), and then kept in petri dishes containing Volvic source water supplemented with 0.3 μg/ml of methylene blue at 28°C or 24°C when slightly delayed development was desirable (all timings in the text refer to the developmental stage at the reference temperature of 28.5°C) (17). A few hours before injection, embryos were dechorionated manually. Larvae were anesthetized with 200 μg/ml tricaine (Sigma-Aldrich) during the injection procedure.

Bacteria. Bacterial strains used in this study were *Listeria innocua* (BUG 499), *L. monocytogenes* wild-type strain EGD (BUG 600), EGD expressing green fluorescent protein (GFP) (BUG 1908), and *L. monocytogenes* isogenic EGD Δ*hly* (BUG 2132) and Δ*actA* (BUG 2140) deletion mutants.

Infections. A 0.5-ml aliquot of a bacterial culture grown overnight was inoculated into 10 ml of brain heart infusion (BHI) liquid medium (Difco) and incubated at 37°C with shaking until an optical density at 600 nm of 0.8 was reached (8×10^8 CFU/ml). Bacteria were then recovered by centrifugation, washed, resuspended in phosphate-buffered saline (PBS) to a concentration of 10^{10} CFU/ml, and kept on ice until the moment of injection. Just before starting the injection, the bacteria were diluted to the appropriate final concentration with PBS containing 0.05% phenol red (Gibco). Anesthetized larvae were microinjected i.v. with 1 to 2 nl of bacterial suspension as described previously (25). The exact inoculum was checked a posteriori by injection in a water drop and plating onto BHI agar. Infected larvae were transferred into individual wells (containing 1 ml of Volvic water in 24-well culture plates), incubated at 28°C (or 33°C as noted), and regularly observed under a stereomicroscope. Infections with a quantified standard dose (~10^3 CFU) were performed six times with wild-type *L. monocytogenes* (i.e., EGD) and three times with every other strain and were found to yield reproducible results provided that the inoculum was checked; survival curves with graded doses as depicted were repeated twice, with similar results.

Measurement of bacterial burden. At the indicated times, animals were anesthetized, rinsed, and collected in 30 μl of sterile water. The animals were lysed in 200 μl of 0.4% Triton X-100–H_2O and homogenized through a 26-gauge needle (five up-and-down sequences). Serial dilutions of the homogenates were plated onto BHI agar, and CFU were enumerated after 48 h of incubation at 37°C; only colonies with the appropriate morphology and color were scored. Statistical analyses of the results were performed by running unpaired Student *t* tests on log values of CFU counts. Experiments were performed twice, with similar results.

Immunohistochemistry. Whole-mount immunohistochemistry was performed using standard zebrafish protocols (39) with the following modifications. Anesthetized animals were fixed overnight at 4°C in 4% methanol-free formaldehyde (Polysciences, Warrington, PA) in PBS. Permeabilization was performed by a 1-h treatment at room temperature with 1 mg/ml collagenase (Sigma). As primary antibodies, rabbit polyclonal antisera that recognize *L. monocytogenes* or *L. innocua* (R11 and R6, respectively), described previously (7), were used at a 1:800 dilution. The secondary antibody used was Cy3-labeled goat anti-rabbit immunoglobulin (Jackson Immunoresearch) diluted 1:500. Images were taken using a fluoIII MZ-16 stereomicroscope (Leica Microsystems, Solms, Germany) equipped with a DS-5Mc camera (Nikon, Tokyo, Japan).

Live imaging. Anesthetized embryos were mounted onto depression slides and imaged as described previously (12, 25), using a Reichert Polyvar2 compound microscope with a 40×/1.00-numerical-aperture or 100×/1.32-numerical-aperture oil objective. DIC and fluorescence images were generated using a three-charge-coupled-device video camera (HVD-20; Hitachi, Leeds, United Kingdom), recorded on miniDV tapes, and later captured with BTVPro software.

Electron microscopy. For standard ultrastructure analyses, dissected tail segments from anesthetized embryos were fixed overnight at 4°C in 2.5% glutaraldehyde in 0.1 M Na cacodylate buffer, postfixed for 1 h in the same buffer containing 1% osmium tetroxide, dehydrated through a graded series of ethanol, and then embedded in an Epon-Araldite resin (33). Thin sections (50 to 70 nm) were cut using a Leica Ultracut-ECT microtome, stained for 4 min with 4% uranyl acetate, and observed under a Jeol (Croissy sur Seine, France) Jem 1010

transmission electron microscope at 80 kV. Digital acquisition was performed with a Keen View camera (Eloise, France).

In order to visualize the actin cytoskeleton, samples were fixed for 40 min at 4°C in a solution containing 1% glutaraldehyde and 1% osmium tetroxide in 0.05 M phosphate buffer (pH 6.3), postfixed in 0.5% uranyl acetate overnight, dehydrated in ethanol, and embedded in Epon as described previously (37).

RESULTS

Zebrafish embryos are susceptible to i.v. *Listeria monocytogenes* infection. We tested the outcome of experimental infection of early zebrafish larvae with *Listeria monocytogenes.* Larvae aged 54 h postfertilization (hpf) were microinjected i.v. near the urogenital opening (Fig. 1A) with wild-type *L. monocytogenes* reference strain EGD and incubated individually at 28°C. A typical inoculum of $\sim 10^3$ EGD bacteria resulted in the death of most larvae within 3 days postinfection (Fig. 1B). In contrast, larvae injected with a comparable inoculum of *Listeria innocua* survived for more than a week, apparently healthy, as evidenced by the fact that almost all larvae developed a swim bladder at the expected age.

Injections with graded inocula (Fig. 1B) indicated that lethality is dose dependent and that under such conditions, the 50% lethal dose (LD_{50}) of *L. monocytogenes* is around 100 CFU, while the LD_{50} of *L. innocua* is more than 3 orders of magnitude higher ($>3 \times 10^4$ CFU).

The progression of the infection was measured using two complementary methods. First, the amount of viable bacteria within inoculated larvae (using an inoculum of $\sim 10^3$ CFU, the dose used throughout the study unless otherwise specified) was measured by plating serial dilutions of ground euthanized animals onto bacterial culture dishes (Fig. 1C). At 1 h postinfection (hpi), only around one-third of the inoculum was recovered as viable bacteria, but thereafter, *L. monocytogenes* numbers strongly increased, reaching 100 times the initial inoculum in 2 days. In contrast, *L. innocua* numbers steadily decreased, even though some viable bacteria persisted for at least 2 days.

Second, infected larvae were subjected to whole-mount immunohistochemistry using *L. monocytogenes*- or *L. innocua*-specific antisera. *nacre* mutants devoid of body melanophores were used; their susceptibility to *L. monocytogenes* infection was similar to that of wild-type zebrafish (not shown). Using this technique, clusters of more than ~10 bacteria were detectable using a fluorescence stereomicroscope (Fig. 1D); smaller groups and single bacteria could be viewed at higher magnifications using wide-field or confocal fluorescence microscopy (not shown). One hour after infection with *L. monocytogenes*, bacterial aggregates were observed mostly in the vicinity of the injection site, whereas single or small groups of bacteria were also scattered all along the caudal hematopoietic tissue (CHT) or over the yolk. One day after inoculation, many bacterial foci could be observed in the CHT and over the yolk sac, and a few were also seen at other places, variable from one larva to the other. By 2 days postinfection, the CHT was massively infected, and large foci were observed at other places, generally in the yolk sac and in a few somites as well as in other seemingly random positions and tissues. For *L. innocua*, the initial distribution was very similar except that almost all bacteria were found in aggregates. Thereafter, scattered, smaller bacterial clusters remained detectable within the CHT for at least 2 days.

In 54-hpf zebrafish larvae, two populations of phagocytes are known to be present: macrophages and granulocytes (24). Many are found within tissues, but a sizable fraction is in contact with the blood flow: most are found in the CHT, a fraction adheres to the walls of the duct of Cuvier (Fig. 1A) or other venous vessels, and a few circulate. The pattern of bacterial distribution observed 1 h after infection suggests that a fraction of the inoculum systematically leaked into the tissues close to the injection site, while the rest became blood borne. However, we wondered whether the fact that bacteria ultimately localize mostly within the CHT could be attributed to the injection being performed there rather than to a preferential trapping of blood-borne bacteria in this region. To answer this question, we tested a different route of i.v. injection, directly into the duct of Cuvier (Fig. 1A), which is a more difficult procedure, as the underlying giant yolk cell is easily injured. Following such injections, a predominant accumulation of bacteria within the CHT was still observed (not shown).

We tested alternative ways to infect the larvae: injections performed directly inside the yolk cell resulted in death faster and at lower doses than i.v. injections; in fact, even *L. innocua* readily killed zebrafish larvae under this condition, although more slowly than *L. monocytogenes* (not shown). On the other hand, the addition of bacteria directly to the water (up to 10^{10} CFU/ml) in which the larvae swim did not result in any detectable pathogenic effect, even with older larvae (up to 6 days postfertilization) with a digestive tract open to the outside environment.

Finally, we also tested the effect of an increase in temperature: following i.v. injections, larvae were incubated at 33°C, the upper limit of the thermal tolerance range of zebrafish. The outcome of the infection was very similar albeit slightly faster (not shown). Of note, previous studies have shown that listeriolysin is still expressed at 30°C although to a lower level than at 37°C (16) and that *Listeria* infection and *actA* expression can occur in S2 *Drosophila* cells cultured at 30°C (28).

Real-time analysis of the early steps of *L. monocytogenes* cell infection in vivo. We took advantage of the transparency of the zebrafish larva to monitor early events of *L. monocytogenes* infection in vivo. To facilitate bacterial detection, we used GFP-expressing *L. monocytogenes* (EGD-GFP) in *nacre* zebrafish larvae. The virulence of these bacteria was comparable to that of parental EGD bacteria (not shown). Anesthetized 54-hpf zebrafish larvae were injected i.v. with EGD-GFP bacteria, laterally mounted onto a depression slide, and imaged by both DIC and fluorescence optics under a compound microscope. Bacterium-phagocyte interactions could be imaged best in the duct of Cuvier. Many free-flowing bacteria were viewed there at first, but all had disappeared within 1 h after injection. This was paralleled by a progressive increase in the number of bacteria that were visible inside phagocytes. Occasionally, it was possible to record a macrophage catching a free bacterium (Fig. 2A): adherence to one of the phagocyte pseudopods was instantaneous and was followed by a slow retraction of the pseudopod and engulfment of the prey. Similar events were recorded following *L. innocua* injection (see Movie S1 in the supplemental material).

Most of the bacterium-containing cells in the duct of Cuvier

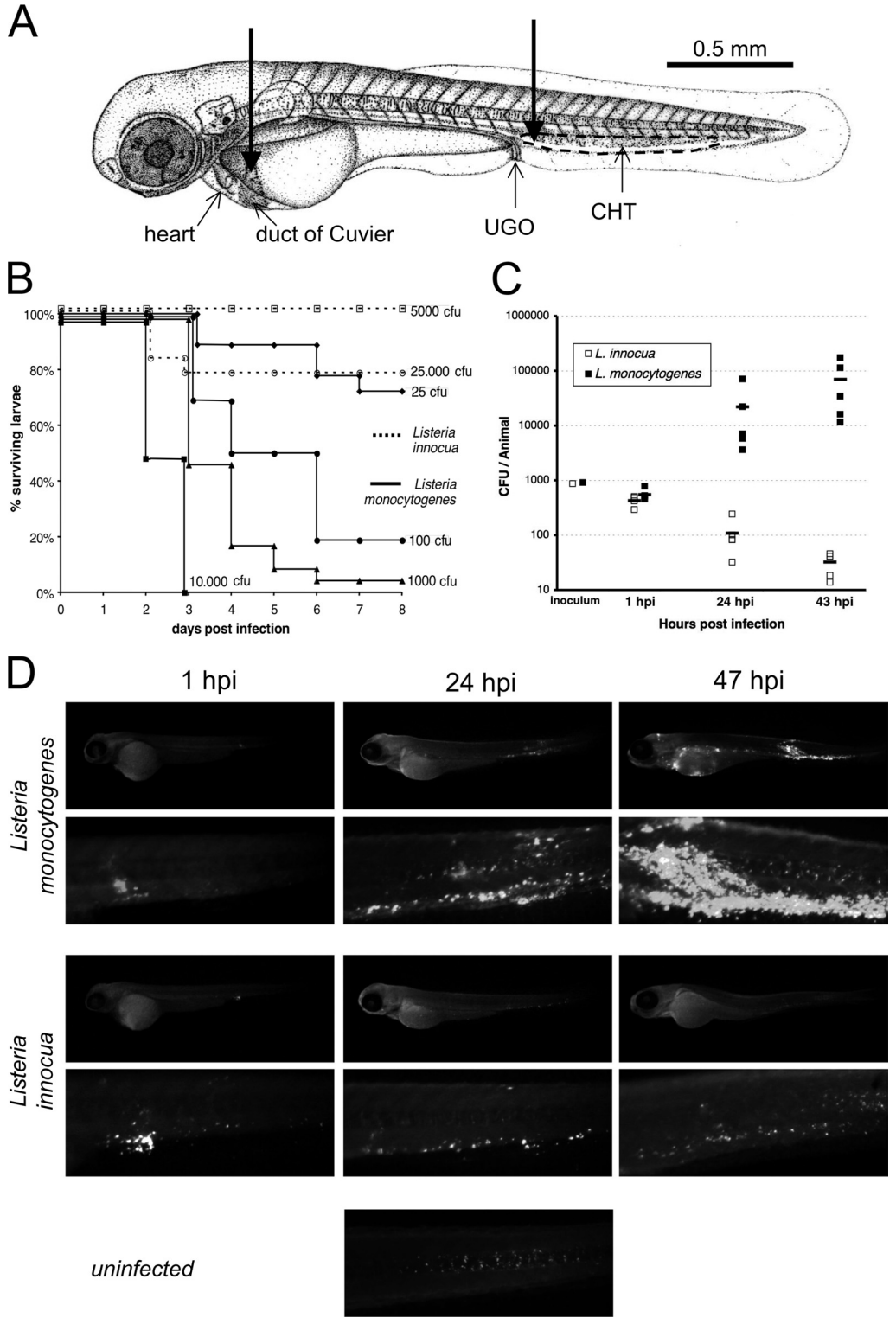

FIG. 1. *Listeria monocytogenes* is virulent following i.v. injection into zebrafish larvae. (A) Injection sites (thick arrows) depicted on a scheme of 60-hpf larva. Most i.v. injections were made in the enlarged venous sinus just caudal to the urogenital opening (UGO). Some were also done directly into the duct of Cuvier, the wide vessel flowing over the yolk. The main hematopoietic organ at this age is the CHT, located between the dorsal aorta and cardinal vein in the ventral tail and delimited here with a dotted line. (B) Survival curves of 54-hpf larvae injected with various doses of *L. monocytogenes* (filled lines) or *L. innocua* (dotted lines) and incubated at 28°C ($n = 16$ to 23 per group). The effective inoculum, quantified a posteriori, fell within the indicated dose ±25%. (C) Enumeration of live bacteria in homogenates from individual larvae at various times postinfection measured by plating onto BHI agar. At days 1 and 2, numbers of CFU were statistically different in *L. monocytogenes*- and *L. innocua*-injected larvae ($P < 10^{-4}$). (D) Distribution of bacteria determined by immunofluorescence at various times postinfection with 10^3 CFU. For each larva, an image of the whole body and a close-up of the tail are shown. The uninfected control reveals nonspecific punctate staining of the notochord; this was easy to tell apart from bacteria by shape, size, and location.

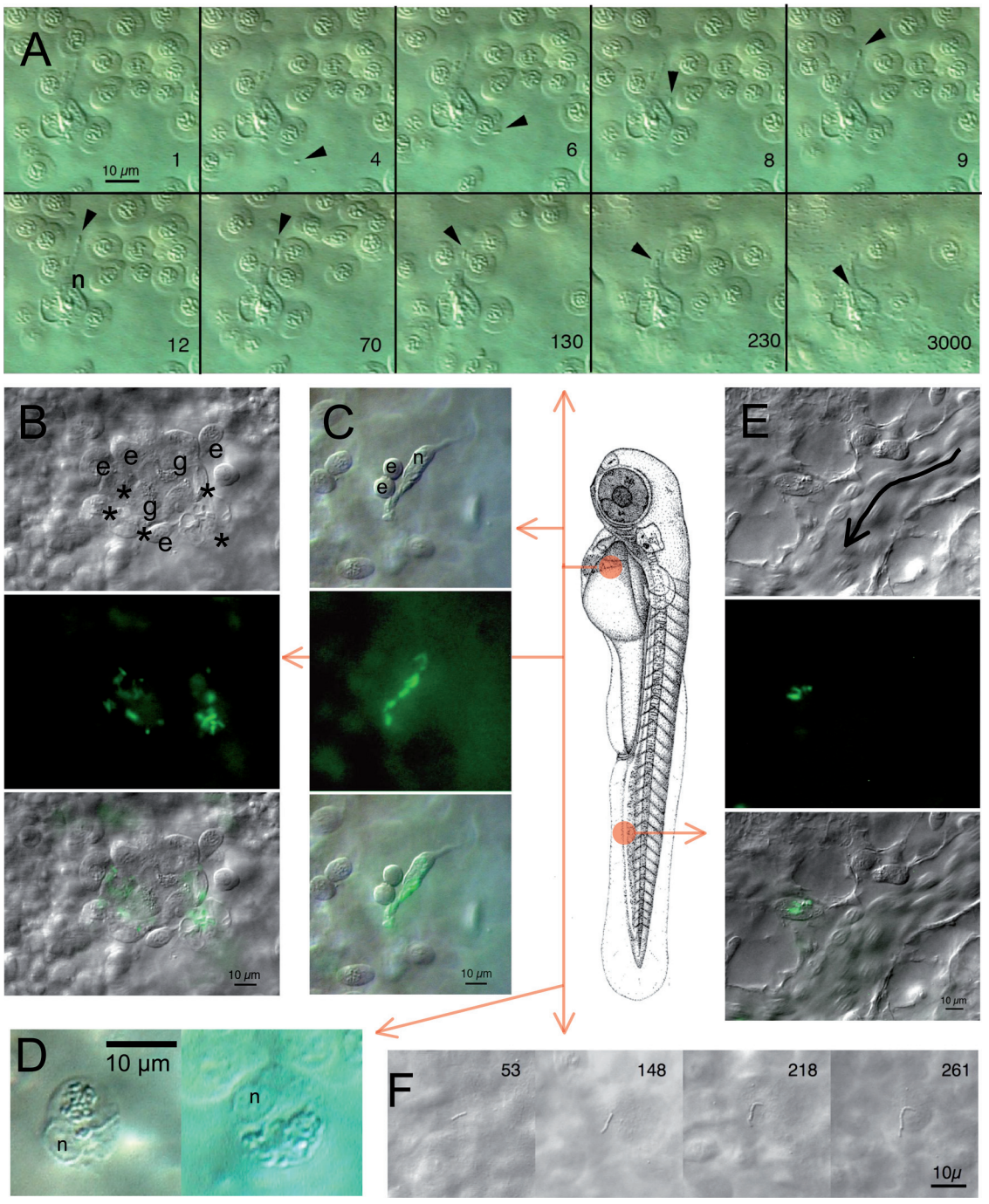

FIG. 2. In vivo microscopic observation of early *Listeria* infection. Larvae at 55 hpf were examined either in the region of the duct of Cuvier (A, B, C, D, and F) or in the CHT (E); the central scheme depicts the location but not the orientation. Observations were performed 1 to 2 h following i.v. injection of GFP-expressing *L. monocytogenes* (A, B, C, E, and F) or of *L. innocua* (D). (A) Phagocytosis of blood-borne *L. monocytogenes* by a macrophage in the duct of Cuvier. Ten frames were extracted from a 1-h DIC movie. The number on lower right corner of each frame indicates time in seconds; time zero starts at around 1 hpi. The position of the bacterium is indicated by the arrowhead, and the nucleus of the macrophage is indicated by an n. Other cells are erythrocytes temporarily trapped due to the pressure of the coverslip on the yolk sac. (B, C, and E) Bacterium-containing cells viewed by DIC (top), fluorescence (middle), or both (bottom). (B) Typical aggregation of cells observed in the duct of Cuvier at 1 hpi, with bacterium-laden macrophages (asterisks), granulocytes that do not appear to contain bacteria (g), and erythrocytes (e). (C) Isolated macrophage observed in the duct of Cuvier, with several internalized bacteria. n indicates its nucleus; a freshly divided pair of erythrocytes (e) is transiently sticking to it. (D) In larvae infected with *L. innocua*, 1 or 2 h after infection, bacteria are found gathered inside a large, single phagosome per macrophage (DIC optics). n indicates the nucleus. (E) Bacterium-containing myeloid cell observed in the CHT near a caudal vein segment where circulating erythrocytes are seen (the direction of flow is indicated by the curved arrow). (F) A few bacteria stick to the endothelium or the yolk cell surface as shown here and can divide extracellularly. The time in minutes postinfection is indicated on each frame.

were observed within small cell aggregates (Fig. 2B). By cell morphology and organelle movements viewed with DIC optics, these aggregates included macrophages, granulocytes, and erythrocytes; bacteria were inside macrophages, but very few, if any, could be seen inside granulocytes. These aggregates appeared quite stable, with no cell leaving or being recruited over several hours of observation. A few isolated macrophages containing bacteria were also observed in every larva (Fig. 2C). Bacteria were seen in several places within the cell, but it was not possible to tell whether they were inside phagosomes or in the cytosol. High-magnification time-lapse recording of one such cell (see Movie S2 in the supplemental material) revealed that the infected cell remained highly motile, while intracellular bacterial motion was also apparent. This cell contains numerous refringent vesicles containing apparently inert material as well as GFP-positive, moving bacteria in a perinuclear region apparently devoid of membranes, suggesting that these bacteria may be in the cytosol rather than in vacuoles. These *L. monocytogenes*-containing macrophages looked strikingly different from those observed for larvae injected with *L. innocua*. In the latter case, macrophages displayed one single, well-delineated phagosome containing dozens of bacteria and appeared immobile (Fig. 2D; see Movie S3 in the supplemental material); this phenotype was very similar to what was previously observed for embryos injected with other gram-positive bacteria, *Bacillus subtilis* (13) and *Staphylococcus aureus* (34).

Observations of the CHT region during the first hours of infection with *L. monocytogenes* revealed many phagocytes containing bacteria adhering to endothelial cells on the luminal side of the complex venous sinusoids. These cells were often isolated (Fig. 2E) or in small groups. Although bacterium-containing leukocytes were more numerous in the CHT than in the duct of Cuvier, they were more difficult to characterize because of the more complex histological context.

While all circulating bacteria had been cleared in less than 1 h after initial injection, some were occasionally found to adhere to endothelial surfaces. In this case, they were dividing extracellularly (Fig. 2F).

Cytosolic infection of macrophages by *L. monocytogenes* in zebrafish larvae. DIC video imaging of EGD-GFP-containing macrophages in zebrafish larvae suggested that, like in mammals, *L. monocytogenes* had the ability to escape from the phagosome and reach the cytosol of macrophages. To demonstrate that such events did occur, we analyzed the CHT of *L. monocytogenes*-infected zebrafish larvae at 3 hpi using transmission electron microscopy (TEM); to increase the number of detectable events, a high inoculum ($\sim 10^4$ CFU) was used.

Almost all bacteria were observed inside leukocytes. Some macrophages unquestionably harbored bacteria within their cytosol (Fig. 3A, with an enlarged view of one bacterium in Fig. 3B). Other bacteria, however, were enclosed within vacuoles, sometimes apparently undergoing degradation (Fig. 3C). Although most bacteria were within macrophages, a few were also seen inside neutrophils (recognizable by their spindle-shaped granules), always in vacuoles and usually degraded (Fig. 3D). A method of staining described previously by Tilney and Portnoy (37) was used in an attempt to determine whether *L. monocytogenes* relies on the polymerization of host actin to propel itself in the cytosol. This was indeed found to occur in zebrafish, as can be seen in Fig. 3E, where a dividing bacterium is seen with a characteristic "comet tail" inside a typical cell protrusion. Although well documented using cell culture, such comet tail-induced protrusions have very rarely been observed for mammalian hosts; in fact, the only comparable published image that we are aware of dates back to a 1972 study of guinea pig (35).

Such protrusions allow *L. monocytogenes* to infect neighboring cells in in vitro mammalian models of infection. This may occur in the zebrafish, as suggested by Fig. 3F, where an endothelial cell distant from the injection site is seen to contain bacteria inside its cytosol (a rare occurrence); this nonprofessional phagocyte may have been infected via protrusions from one of the numerous *L. monocytogenes*-containing macrophages found in its microenvironment. Alternatively, free bacteria in the blood might have directly adhered to and entered this cell.

Listeriolysin and ActA are *L. monocytogenes* virulence factors in zebrafish. In mammalian *L. monocytogenes* infections, escape of the phagosome and subsequent cytosolic movement are mediated by listeriolysin and ActA, respectively. Our TEM observations prompted us to investigate whether listeriolysin-deficient (Δ*hly*) and *actA*-deficient (Δ*actA*) isogenic *L. monocytogenes* mutants would be attenuated in the zebrafish model.

When microinjected intravenously in 54-hpf zebrafish larvae, Δ*hly* mutants were found to be fully attenuated, with no practically injectable dose leading to the death of larvae (Fig. 4A). As with *L. innocua*, counts of Δ*hly* bacteria in infected larvae were found to decline progressively, with a fraction nevertheless being able to persist for at least 2 days (Fig. 4B).

The Δ*actA* mutant was also attenuated but to a lesser extent that the Δ*hly* mutant. The LD_{50} of the Δ*actA* mutant was approximately 3×10^3 CFU/larva, i.e., a 1- to 2-log-fold increase over wild-type *L. monocytogenes* (Fig. 4A). Quantification of bacteremia in Δ*actA* mutant-infected larvae revealed a higher dispersion of the results, with some larvae clearly controlling bacterial numbers, while others became overwhelmed by bacterial proliferation (Fig. 4B).

Δ*hly* mutant- or Δ*actA* mutant-infected larvae were also observed microscopically in the early stages of infection. While the phagocytes of Δ*actA* mutant-infected larvae looked similar to those of wild-type *L. monocytogenes*-infected animals, observations of Δ*hly* mutant-infected larvae were strongly reminiscent of *L. innocua*-infected larvae. Most notably, a few hours after injection, as one would have expected from a mutant unable to escape the vacuolar compartment, macrophages were found to harbor large phagosomes containing dozens of bacteria (Fig. 4C).

DISCUSSION

We describe here the successful establishment of a new *Listeria monocytogenes* infection model system, the larval zebrafish, which allows a detailed in vivo real-time analysis of host-pathogen interactions. Following i.v. injection in 54-hpf zebrafish larvae, *L. monocytogenes* bacteria establish a systemic infection at 28°C and multiply in the host, resulting in death in about 3 days (Fig. 1). Most bacterial proliferation appears to take place intracellularly, although we have occasionally observed an extracellular proliferation of *L. monocytogenes* adhering to endothelium (Fig. 2F). Similar in this respect to other

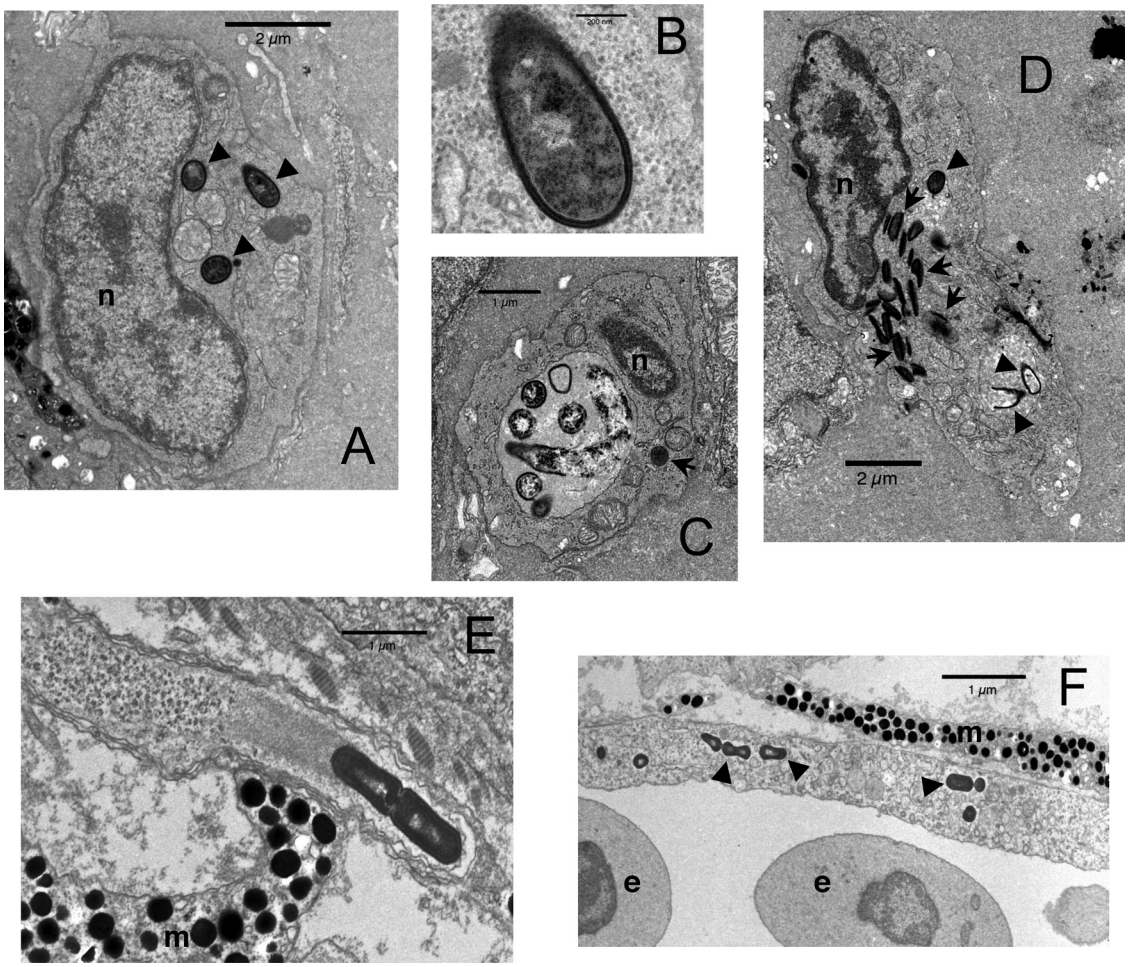

FIG. 3. Ultrastructural analysis of *L. monocytogenes* infection of zebrafish larvae. (A to D) Standard staining at 3 hpi. (E and F) Tilney staining at 24 hpi. (A) Macrophage containing three intracytoplasmic bacteria (arrowheads). (B) Close-up of one of these bacteria showing the absence of any membrane between the bacterial cell wall and cytosol. (C) Macrophage with a large phagosome containing bacteria at various stages of degradation. The dark object in the cytosol, indicated by an arrow, does not harbor a cell wall and is probably a fat globule. (D) Neutrophilic granulocyte, identifiable by its typical spindle-shaped granules (arrows), with at least two killed bacteria (bottom arrowheads) within a phagosome and a third one probably still alive (top arrowhead) in another phagosome. (E) Typical cell protrusion containing a dividing bacterium propelled by an actin tail. (F) Infected endothelial cell, with some bacteria indicated by arrowheads and vessel lumen on the bottom of the image. n, nucleus; m, melanophore; e, erythrocyte.

bacteria such as *Escherichia coli*, *B. subtilis*, *Salmonella* Typhimurium, or *Staphylococcus aureus* (13, 34, 38), pathogenic *L. monocytogenes* or its nonpathogenic relative *L. innocua* is quickly cleared from the bloodstream by phagocytes, notably macrophages to which they readily stick; they are then internalized within a few minutes (Fig. 2A; see Movie S1 in the supplemental material). However, while *L. innocua* bacteria accumulate inside large phagosomes (Fig. 2D; see Movie S3 in the supplemental material), where they are presumably killed and degraded, events take a radically different course with *L. monocytogenes*: while a fraction of internalized *L. monocytogenes* bacteria stay within vacuoles, where they are destroyed, some manage to escape from the phagosome and invade the cytosol of macrophages (Fig. 3A to D). The bacteria can then propel themselves inside the cytosol by polymerizing host actin and can be found in cellular protrusions that could allow them to infect neighboring cells (Fig. 3E and F). Similar events are known to be critically important for the virulence of *L. monocytogenes* in mammalian hosts; we show here that they involve the same virulence factors in the zebrafish, since listeriolysin and *actA* mutants are attenuated in zebrafish (Fig. 4).

This zebrafish host model of *L. monocytogenes* infection displays several very interesting features. The fact that major virulence mechanisms and genes are conserved with mammalian systems indicates that the zebrafish larva constitutes a relevant model of human infection for at least some of its aspects, notably host-phagocyte interactions. Their remarkable optical accessibility allowed us to image *Listeria* phagocytosis in vivo (Fig. 2A; see Movie S1 in the supplemental material), an achievement that has never been accomplished for rodent host models. Live imaging of some bacterium-containing macrophages observed as soon as 1 or 2 hpi is strongly suggestive of cytosolic infection (Fig. 2C; see Movie S2 in the supplemental material). It may become possible in the future to observe *L. monocytogenes* phagosome escape and actin comet nucleation in vivo by developing new transgenic zebrafish lines. A

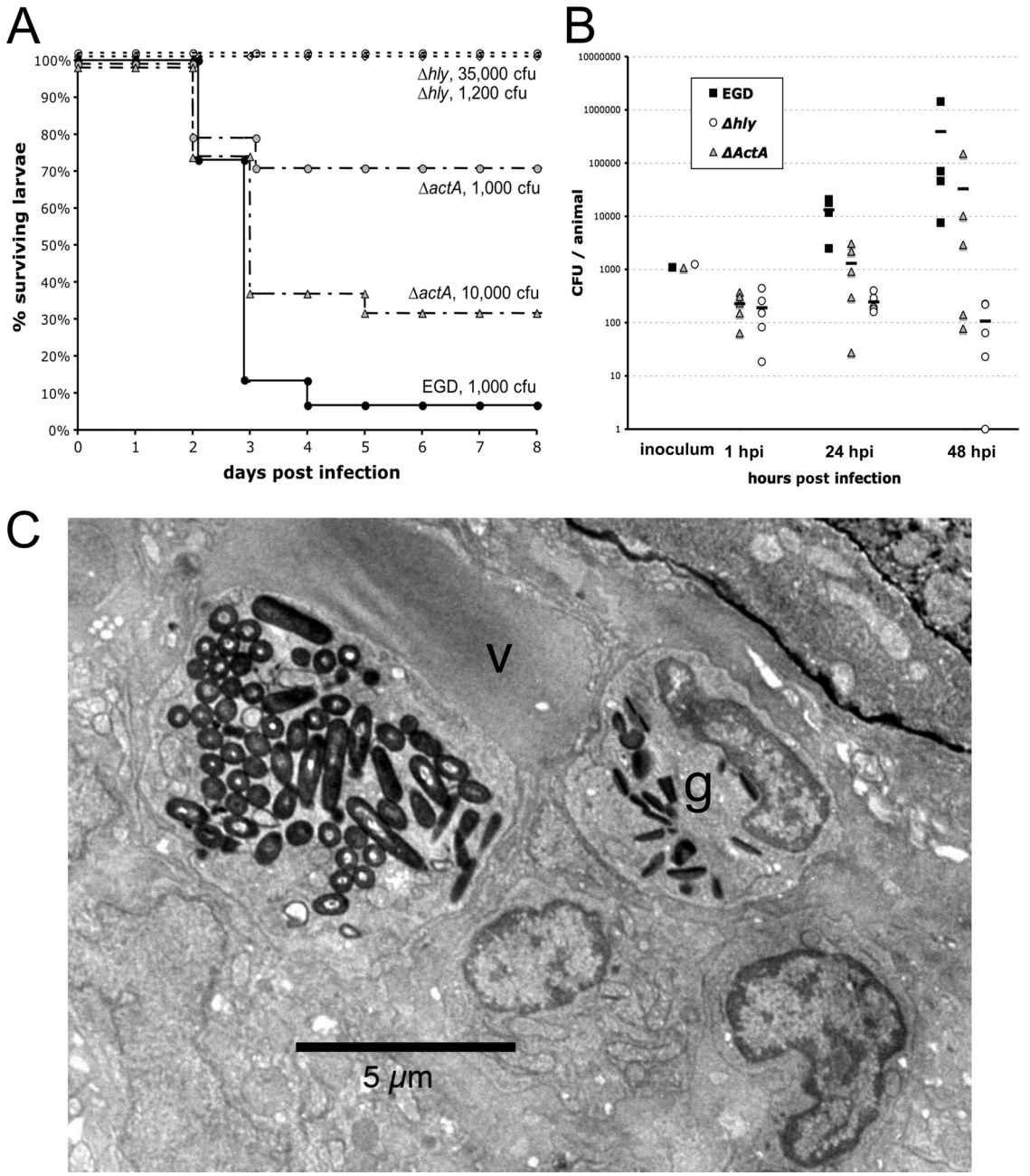

FIG. 4. Listeriolysin and ActA are virulence factors for *L. monocytogenes* in the zebrafish model. (A) Survival curve of zebrafish larvae infected i.v. with wild-type *L. monocytogenes* (EGD) or with Δ*actA* or Δ*hly* EGD mutants at various doses and incubated at 28°C ($n = 15$ to 24 per group). (B) Enumeration of bacteria inside whole larvae at various time points following i.v. infection. Load was not measured at 1 hpi in EGD-infected larvae in this experiment (see Fig. 1C for a similar measurement). At days 1 and 2, CFU numbers were statistically different when Δ*hly* mutant- and EGD-injected larvae were compared ($P < 10^{-3}$) or, less significantly, when Δ*actA* mutant- and EGD-injected larvae were compared ($P < 0.05$). (C) TEM image of a typical macrophage in a zebrafish infected with the Δ*hly* mutant at 3 hpi, with a huge phagosome containing many bacteria. The nucleus is not visible in this plane. The macrophage is in direct contact with the lumen of the vein (v). A bacterium-free neutrophilic granulocyte (g) is also visible in its vicinity.

transgenic zebrafish expressing a cytosolic form of the *L. monocytogenes*-binding cell wall-binding domain phage protein fused to a fluorescent reporter would allow the real-time detection of phagosome escape, as *L. monocytogenes* attaining the cytosolic compartment would become brightly stained (11), while a second transgene coding for actin fused to a complementary fluorophore would simultaneously allow the observation of actin comets (2). By combining such approaches with the relatively simple techniques of gene knockdown and overexpression available for zebrafish larvae, the interactions between *L. monocytogenes* and host phagocytes in vivo become amenable to analysis at an unprecedented level of spatiotemporal resolution.

Of note, although we could also infect and kill larvae with *L. monocytogenes* by injections in yolk, which are much easier than i.v. injections and thus more suitable for high-throughput screening purposes, this approach appears to be much less useful for the study of virulence mechanisms, since even normally nonpathogenic bacteria such as *L. innocua* become lethal under such conditions. This result, which mirrors previously reported observations of attenuated *S.* Typhimurium (38), nonpathogenic *E. coli* or *B. subtilis* (J.-P. Levraud and P. Herbomel, unpublished observations), or minuscule amounts of *S. aureus* (34), is unfortunate but hardly surprising, as such an infection route constitutes, in fact, a direct injection into the cytosol of the giant yolk cell, a highly nutritive environment that is inaccessible to leukocytes.

In humans, the ability of *L. monocytogenes* to cross host barriers (intestine, BBB, or placenta) is of great importance for its virulence. However, in our preliminary experiments, *L. monocytogenes* was apparently not able to cross the larval zebrafish intestinal mucosa efficiently: bath exposure of 5- or 6-day-postfertilization larvae, which already possess a functional digestive system and readily swallow surrounding water, did not result in detectable pathology (our unpublished data). Infection of human enterocytes is critically dependent on interactions between host E-cadherin and the virulence factor InlA; a single difference in the 16th amino acid of E-cadherin between human and mouse has been shown to be critical for the absence of entry of *L. monocytogenes* in mouse enterocytes (22). Although zebrafish E-cadherin harbors a proline in this position, it may not interact with InlA, as it is otherwise much more divergent from its human counterpart than the mouse protein; however, this remains to be tested. In this case, it would be interesting to generate transgenic zebrafish expressing human E-cadherin in the intestine, similar in this respect to iFABP-Ecad mice (23); such fish may be susceptible to oral *L. monocytogenes* infection and thus allow real-time in vivo imaging of gut crossing by *L. monocytogenes*. In addition, at the stages used here, the BBB is not yet formed; late larvae aged at least 2 weeks would have to be used for a fully formed BBB (15; E. Colucci-Guyon and K. Kissa, unpublished data). This may be worth testing in the future, even though optical accessibility and genetic tractability are not as good at these late stages of development as in early larvae; it would also pave the way for an analysis of adaptive immunity to *L. monocytogenes* in zebrafish, which become fully immunocompetent by 4 to 6 weeks of age (20).

The occasional observation of *L. monocytogenes* inside endothelial cells (Fig. 3F) suggests that some barrier crossing does occur in the larval zebrafish model, and this fact deserves more investigation. The most likely route of infection of endothelial cells appears to be through protrusions emerging from infected macrophages; nevertheless, the not-so-uncommon observation of *L. monocytogenes* adhering to vascular walls (Fig. 2F and data not shown) also suggests the possibility of direct internalization by endothelial cells, which could also be relevant to mammalian infections.

Another line of investigation worth following in this system relates to the interactions between infected macrophages and neutrophils. In our in vivo DIC observations, neutrophils were rarely seen to contain bacteria; TEM analysis revealed the presence of a few killed bacteria inside some neutrophil vacuoles but no bacteria in their cytosol. Thus, it seems likely that, just like in mammals, zebrafish neutrophils may be much more toxic to *L. monocytogenes* than resting macrophages, killing engulfed bacteria very quickly and not giving them the chance to escape the phagosome. In mice, neutrophils have been shown to play a very important role in defense against *L. monocytogenes* i.v. infections, especially in the liver (4), and it was previously argued that they act not by directly destroying free bacteria but by internalizing bacteria trapped on the surface of Küpffer cells, which in turn engulf the neutrophils (10). We have frequently observed neutrophils in close contact with infected macrophages (Fig. 2B and data not shown); it remains to be determined whether and how they play a major role in defense against *L. monocytogenes* in zebrafish.

In summary, we show in this study that the zebrafish larva represents a very instrumental new host for the analysis of *Listeria monocytogenes* infection. Interactions between bacteria and host phagocytes can be imaged at high resolution in vivo from the earliest stages, and this model should prove useful for the understanding of many events that until now could only be inferred from in vitro analysis.

ACKNOWLEDGMENTS

We thank Marie-Christine Prevost for supervision of ultrastructural microscopy, Valérie Briolat for management of the fish facility, Emma Colucci-Guyon for many helpful discussions and sharing of unpublished data, Edith Gouin for the generation of BUG 1908, the students of the microbiology general course of Pasteur (2003 to 2004) for the generation of BUG 2132 and BUG 2140, David Parichy for the gift of the *nacre* mutants, and the team of the Imaging Facility of Institut Pasteur.

Olivier Disson has been supported by grants from Inserm and the Fondation pour la Recherche Médicale. Pascale Cossart is a Howard Hughes Medical Institute international research scholar. This work has been funded by institutional grants from the Institut Pasteur, Inserm, and CNRS.

REFERENCES

1. **Aoshi, T., B. H. Zinselmeyer, V. Konjufca, J. N. Lynch, X. Zhang, Y. Koide, and M. J. Miller.** 2008. Bacterial entry to the splenic white pulp initiates antigen presentation to CD8+ T cells. Immunity **29:**476–486.
2. **Choidas, A., A. Jungbluth, A. Sechi, J. Murphy, A. Ullrich, and G. Marriott.** 1998. The suitability and application of a GFP-actin fusion protein for long-term imaging of the organization and dynamics of the cytoskeleton in mammalian cells. Eur. J. Cell Biol. **77:**81–90.
3. **Clay, H., J. M. Davis, D. Beery, A. Huttenlocher, S. E. Lyons, and L. Ramakrishnan.** 2007. Dichotomous role of the macrophage in early Mycobacterium marinum infection of the zebrafish. Cell Host Microbe **2:**29–39.
4. **Conlan, J. W., and R. J. North.** 1994. Neutrophils are essential for early anti-Listeria defense in the liver, but not in the spleen or peritoneal cavity, as revealed by a granulocyte-depleting monoclonal antibody. J. Exp. Med. **179:**259–268.
5. **Davis, J., H. Clay, J. Lewis, N. Ghori, P. Herbomel, and L. Ramakrishnan.** 2002. Real-time visualization of *Mycobacterium*-macrophage interactions leading to initiation of granuloma formation in zebrafish embryos. Immunity **17:**693–702.
6. **Disson, O., S. Grayo, E. Huillet, G. Nikitas, F. Langa-Vives, O. Dussurget, M. Ragon, A. Le Monnier, C. Babinet, P. Cossart, and M. Lecuit.** 2008. Conjugated action of two species-specific invasion proteins for fetoplacental listeriosis. Nature **455:**1114–1118.
7. **Dramsi, S., S. Lévi, A. Triller, and P. Cossart.** 1998. Entry of *Listeria monocytogenes* into neurons occurs by cell-to-cell spread: an in vitro study. Infect. Immun. **66:**4461–4468.
8. Reference deleted.
9. **Gaillard, J. L., P. Berche, J. Mounier, S. Richard, and P. Sansonetti.** 1987. In vitro model of penetration and intracellular growth of *Listeria monocytogenes* in the human enterocyte-like cell line Caco-2. Infect. Immun. **55:**2822–2829.
10. **Gregory, S., and E. Wing.** 2002. Neutrophil-Kupffer cell interaction: a critical component of host defenses to systemic bacterial infections. J. Leukoc. Biol. **72:**239–248.

11. **Henry, R., L. Shaughnessy, M. J. Loessner, C. Alberti-Segui, D. E. Higgins, and J. A. Swanson.** 2006. Cytolysin-dependent delay of vacuole maturation in macrophages infected with Listeria monocytogenes. Cell. Microbiol. **8:**107–119.
12. **Herbomel, P., and J. Levraud.** 2005. Imaging early macrophage differentiation, migration, and behaviors in live zebrafish embryos. Dev. Hematopoiesis **105:**199–214.
13. **Herbomel, P., B. Thisse, and C. Thisse.** 1999. Ontogeny and behaviour of early macrophages in the zebrafish embryo. Development **126:**3735–3745.
14. **Huss, H. H., L. V. Jorgensen, and B. F. Vogel.** 2000. Control options for Listeria monocytogenes in seafoods. Int. J. Food Microbiol. **62:**267–274.
15. **Jeong, J. Y., H. B. Kwon, J. C. Ahn, D. Kang, S. H. Kwon, J. A. Park, and K. W. Kim.** 2008. Functional and developmental analysis of the blood-brain barrier in zebrafish. Brain Res. Bull. **75:**619–628.
16. **Johansson, J., P. Mandin, A. Renzoni, C. Chiaruttini, M. Springer, and P. Cossart.** 2002. An RNA thermosensor controls expression of virulence genes in Listeria monocytogenes. Cell **110:**551–561.
17. **Kimmel, C., W. Ballard, S. Kimmel, B. Ullmann, and T. Schilling.** 1995. Stages of embryonic development of the zebrafish. Dev. Dyn. **203:**253–310.
18. **Kocks, C., E. Gouin, M. Tabouret, P. Berche, H. Ohayon, and P. Cossart.** 1992. L. monocytogenes-induced actin assembly requires the actA gene product, a surface protein. Cell **68:**521–531.
19. **Kurz, C. L., and J. J. Ewbank.** 2007. Infection in a dish: high-throughput analyses of bacterial pathogenesis. Curr. Opin. Microbiol. **10:**10–16.
20. **Lam, S., H. Chua, Z. Gong, T. Lam, and Y. Sin.** 2003. Development and maturation of the immune system in zebrafish, Danio rerio: a gene expression profiling, in situ hybridization and immunological study. Dev. Comp. Immunol. **28:**9–28.
21. **Lecuit, M.** 2007. Human listeriosis and animal models. Microbes Infect. **9:**1216–1225.
22. **Lecuit, M., S. Dramsi, C. Gottardi, M. Fedor-Chaiken, B. Gumbiner, and P. Cossart.** 1999. A single amino acid in E-cadherin responsible for host specificity towards the human pathogen Listeria monocytogenes. EMBO J. **18:**3956–3963.
23. **Lecuit, M., S. Vandormael-Pournin, J. Lefort, M. Huerre, P. Gounon, C. Dupuy, C. Babinet, and P. Cossart.** 2001. A transgenic model for listeriosis: role of internalin in crossing the intestinal barrier. Science **292:**1722–1725.
24. **Le Guyader, D., M. J. Redd, E. Colucci-Guyon, E. Murayama, K. Kissa, V. Briolat, E. Mordelet, A. Zapata, H. Shinomiya, and P. Herbomel.** 2008. Origins and unconventional behavior of neutrophils in developing zebrafish. Blood **111:**132–141.
25. **Levraud, J., E. Colucci-Guyon, M. Redd, G. Lutfalla, and P. Herbomel.** 2008. In vivo analysis of zebrafish innate immunity. Innate Immun. **415:**337–363.
26. **Lister, J., C. Robertson, T. Lepage, S. Johnson, and D. Raible.** 1999. nacre encodes a zebrafish microphthalmia-related protein that regulates neural-crest-derived pigment cell fate. Development **126:**3757–3767.
27. **Mackaness, G. B.** 1962. Cellular resistance to infection. J. Exp. Med. **116:**381–406.
28. **Mansfield, B. E., M. S. Dionne, D. S. Schneider, and N. E. Freitag.** 2003. Exploration of host-pathogen interactions using Listeria monocytogenes and Drosophila melanogaster. Cell. Microbiol. **5:**901–911.
29. **Mengaud, J., H. Ohayon, P. Gounon, R. M. Mege, and P. Cossart.** 1996. E-cadherin is the receptor for internalin, a surface protein required for entry of L. monocytogenes into epithelial cells. Cell **84:**923–932.
30. **Menudier, A., F. Rougier, and C. Bosgiraud.** 1996. Comparative virulence between different strains of Listeria in zebrafish (*Brachydanio rerio*) and mice. Pathol. Biol. **44:**783–789.
31. Reference deleted.
32. **Pamer, E. G.** 2004. Immune responses to Listeria monocytogenes. Nat. Rev. Immunol. **4:**812–823.
33. **Pichon, C., C. Hechard, L. du Merle, C. Chaudray, I. Bonne, S. Guadagnini, A. Vandewalle, and C. Le Bouguenec.** 2009. Uropathogenic Escherichia coli AL511 requires flagellum to enter renal collecting duct cells. Cell. Microbiol. **11:**616–628.
34. **Prajsnar, T. K., V. T. Cunliffe, S. J. Foster, and S. A. Renshaw.** 2008. A novel vertebrate model of Staphylococcus aureus infection reveals phagocyte-dependent resistance of zebrafish to non-host specialized pathogens. Cell. Microbiol. **10:**2312–2325.
35. **Racz, P., K. Tenner, and E. Mérö.** 1972. Experimental Listeria enteritis. I. An electron microscopic study of the epithelial phase in experimental Listeria infection. Lab. Investig. **26:**694–700.
36. **Shen, Y., M. Naujokas, M. Park, and K. Ireton.** 2000. InIB-dependent internalization of Listeria is mediated by the Met receptor tyrosine kinase. Cell **103:**501–510.
37. **Tilney, L. G., and D. A. Portnoy.** 1989. Actin filaments and the growth, movement, and spread of the intracellular bacterial parasite, Listeria monocytogenes. J. Cell Biol. **109:**1597–1608.
38. **van der Sar, A., R. Musters, F. van Eeden, B. Appelmelk, C. Vandenbroucke-Grauls, and W. Bitter.** 2003. Zebrafish embryos as a model host for the real time analysis of *Salmonella typhimurium* infections. Cell. Microbiol. **5:**601–611.
39. **Westerfield, M.** 1993. The zebrafish book. A guide for the laboratory use of zebrafish (*Brachydanio rerio*). University of Oregon Press, Eugene.
40. **Yano, T., S. Mita, H. Ohmori, Y. Oshima, Y. Fujimoto, R. Ueda, H. Takada, W. E. Goldman, K. Fukase, N. Silverman, T. Yoshimori, and S. Kurata.** 2008. Autophagic control of Listeria through intracellular innate immune recognition in Drosophila. Nat. Immunol. **9:**908–916.

Editor: A. J. Bäumler